


# Corrosion degradation of aluminium alloys using a computational framework

Zaigham Saeed TOOR <sup>\*</sup>, Muhammad Moaaz ZAFAR

Department of Materials Science and Engineering, Institute of Space Technology, Islamabad, Pakistan

\*Corresponding author: [zaighamtoor93@gmail.com](mailto:zaighamtoor93@gmail.com)

## Keywords

corrosion  
numerical analysis  
aluminium alloys  
degradation

## History

Received: 22-10-2022

Revised: 20-12-2022

Accepted: 24-12-2022

## Abstract

The paper describes the corrosion based degradation of aluminium alloys using an analytical and numerical framework. The corrosion rate was calculated using analytical equations for aluminium sheets subjected to a corrodent. Parametric analysis for the pit morphology, diameter, depth and distribution on the plate was conducted using finite element analysis. A comparison between elliptical and circular pits of the same area was also made for stress magnification using numerical analysis. It was observed that the stress generated at constant load when a specimen corrodes due to pitting is directly proportional to the pit diameter and pit depth. Zigzag pit morphologies due to the combined effect of mechanical degradation and corrosion have the highest stress at the corners of the pattern, while circular pits have the highest stress at the centre of the pit. The zigzag pit morphology has more detrimental effects than circular pits. For multiple distributed pits, the pits closer to the specimen edges exhibit higher stress values than those near the centre of the specimen. The effect of multiple or quantitatively increased number of pits having smaller geometric properties has a more detrimental effect than a single pit with larger geometric attributes.

## 1. Introduction

Material degradation and corrosion have been an area of serious concern in almost all reputed engineering areas like aerospace engineering, civil engineering, industrial engineering, etc. Uniform corrosion and pitting corrosion are common and severe types of corrosion that damage metallic engineering structures [1-2]. The corrosion damage gets augmented with the applied loads resulting in stress magnification due to both the geometric defect created by corrosion and the load concentration on the reduced area as in the case of tensile stress in stress corrosion cracking (SCC) [3-5]. There are different mathematical models and equations which can help in the calculation of the corrosion rate on a specified specimen against a particular corrodent [6,7]. This can aid the engineers to predict the service life of the

component and calculating the reduced geometric attributes such as thickness. Another way to assess corrosion durability is to conduct accelerated or long-term corrosion testing of standardised coupons subjected to the corrosive environment and then analyse their response to electric potential known as potential dynamic curves [8].

The limitations of corrosion testing are focused on the fact that these tests are conducted on coupons and not full-scale components [9]. Secondly, they require extensive testing time. Thirdly, they do not exhibit stress distribution and concentration due to the degradation of material or structure under constant load. Most importantly, the service life of any component subjected to corrosion cannot be directly predicted using these tests. From the engineering perspective, it is detrimental to analyse the behaviour of a component when it starts corroding in service [10]. Numerical modelling provides an efficient and effective manner to study how the stress distribution and concentration in a component will



This work is licensed under a Creative Commons Attribution-NonCommercial 4.0 International (CC BY-NC 4.0) license

vary once it corrodes by introducing the corroded morphology in the specimen or component using computer-aided design (CAD) [11-13]. The CAD model is subjected to the desired loading conditions in terms of clamping and pressures. The model is then discretised into small elements called meshing and the results are compared with literature or with neat specimens for qualitative analysis [14-17].

This research has calculated the corrosion rate on an aluminium sheet (age hardened aluminium-copper alloy AA 2219) subjected to a corrodent to analyse the reduction in its thickness, followed by a numerical analysis of thickness reduction, pit morphology and distribution introduced in the specimens to analyse the stress distribution and concentration under constant load.

## 2. Methodology

To calculate the effect of uniform corrosion, it was assumed that the surface of desired aluminium sheet is immersed in 3.5 wt. % NaCl solution. The corrosion rate in mils per year (mpy) is calculated by the following relationship:

$$V_{\text{corr}} = \frac{I_{\text{corr}} K E_w}{\rho A}, \quad (1)$$

where  $V_{\text{corr}}$  is the corrosion rate (calculated value is 0.244 mpy),  $I_{\text{corr}}$  is the corrosion current density calculated from potentiodynamic polarization (PDP) curves ( $I_{\text{corr}} = 0.508 \mu\text{A}/\text{cm}^2$ ),  $K$  is the constant for corrosion rate unit as per ASTM standard G102 ( $K = 1.288 \times 10^5 \text{ mpy A}^{-1} \text{ cm}$ ),  $E_w$  is the equivalent weight for the specific aluminium alloy with respect to sample volume ( $E_w = 10.6 \text{ g}$ ),  $\rho$  is the density of a specific aluminium alloy ( $\rho = 2.84 \text{ g}/\text{cm}^3$ ) and  $A$  is the area (sheet length  $\times$  sheet width) of the sample ( $A = 1 \text{ cm}^2$ ).

It is assumed that such pits will be generated against prolonged corrosion of the sheets as per the calculated corrosion rate. Based on this assumption, the pits of a definite geometry are modelled and analysed in the aluminium sheets using FEM as also available in the literature. It is assumed that based on the calculated corrosion rate of 0.244 mpy, the pit formation will start and ultimately reach a circular form i.e. in close approximation to a hole or circle. Therefore for model simplification, elliptical and circular pits are already modelled in the structure before analysing the effect of load [17-20]. The numerical modelling of the aluminium plate was carried out as per the material properties and dimensions mentioned in Tables 1 and 2, respectively.

**Table 1.** Material properties

Property	Value
Density, $\text{g}/\text{cm}^3$	2.84
Modulus of elasticity, GPa	74
Poisson's ratio	0.3
Yield strength, MPa	320

**Table 2.** Model dimensions

Parameter	Value, mm
Sheet length	10
Sheet width	10
Sheet thickness	0.5
Pit depth	0.1 – 0.3
Circular pit diameter	0.2 – 0.4
Elliptical pit diameter	$1.6 \times 0.1 / 0.8 \times 0.2$

The plate was clamped from one end, while the other end was subjected to a tensile load of 10 N as shown in Figure 1. Features and parametric variations in terms of pit diameter, depth, morphology, and distribution were added using computer-aided drafting (CAD) [18,19]. Solid hexahedral elements were used for the meshing of the models and the mesh was refined near the pits or corroded areas for accurate results as shown in Figure 2.

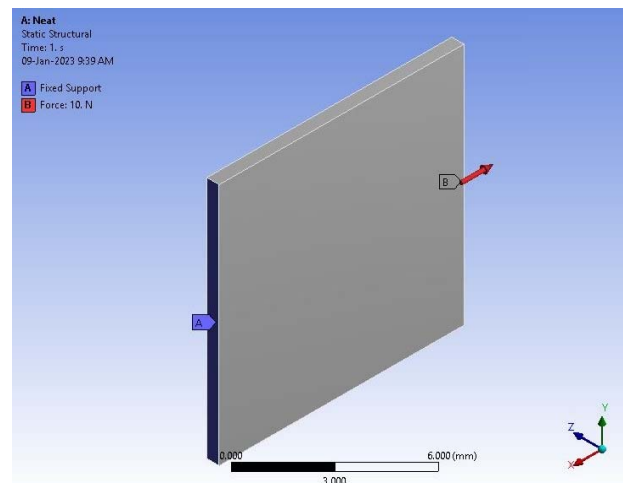


**Figure 1.** Loading conditions of the plate

In order to conduct model calibration and validation, the mesh was refined by taking output values of stress and deformation against the aforementioned boundary conditions. Once no significant variation was observed upon further mesh refinement and the results were found to be in agreement with their analytical counterparts, the element size was then fixed as shown in Figures 3 and 4, respectively.

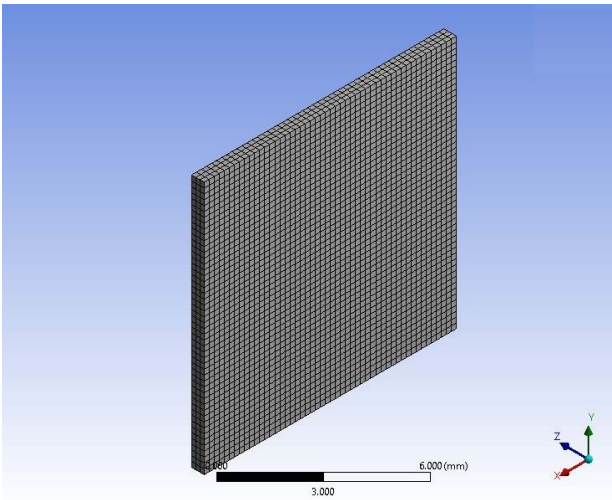


Figure 2. Meshed neat specimen

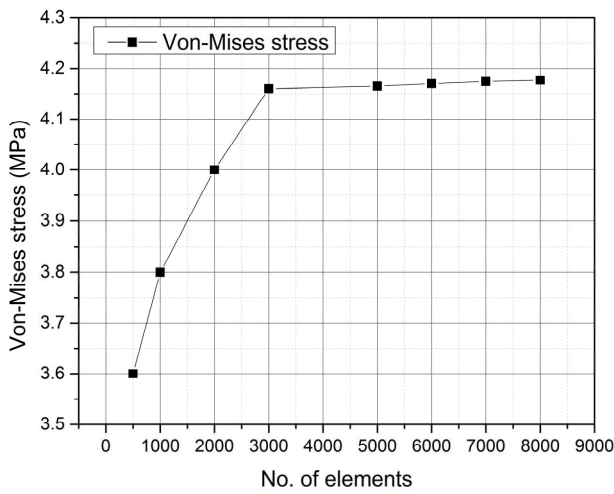


Figure 3. Mesh sensitivity for stress

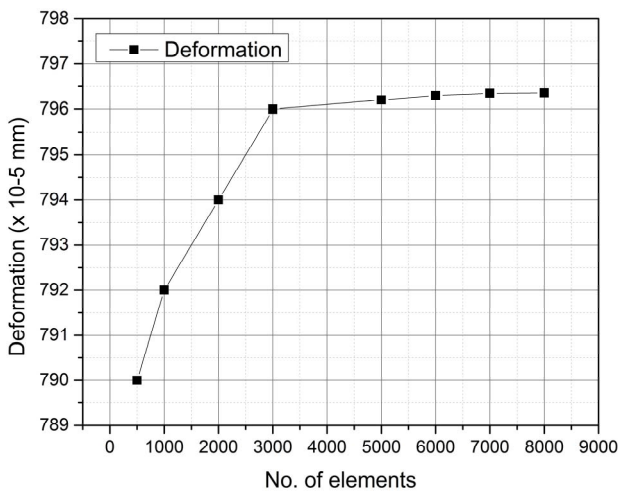


Figure 4. Mesh sensitivity for deformation

### 3. Results and discussion

Figure 5 represents the stress distribution on the neat sample. The highest stress value was observed in the corners of the clamped side, while the remaining stress was uniformly distributed on the plate cross-section normal to the direction of the applied load.

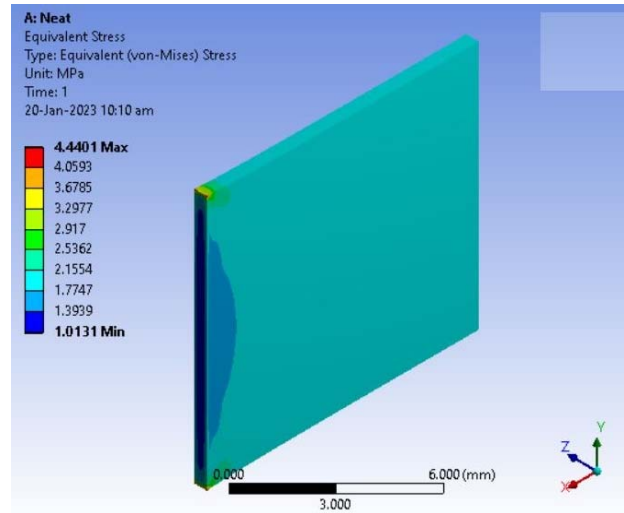


Figure 5. Stress distribution for the neat sample at 0.5 mm plate thickness

Figure 6 represents the effect of pit depth on the stress generated in the specimen. A linear trend between the pit depth and the correspondingly generated stress was observed. Figure 7 represents the stress distribution on the pit sample. The highest stress value was observed to be concentrated at the centre of the pit, indicated by the red colour, while the value of stress decreases upon moving away from the pit.

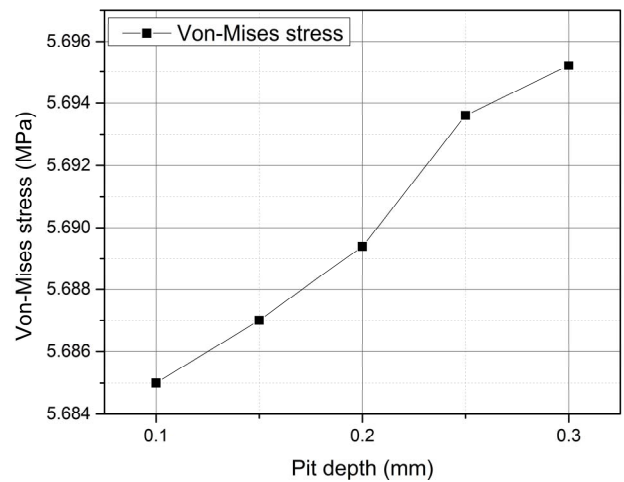
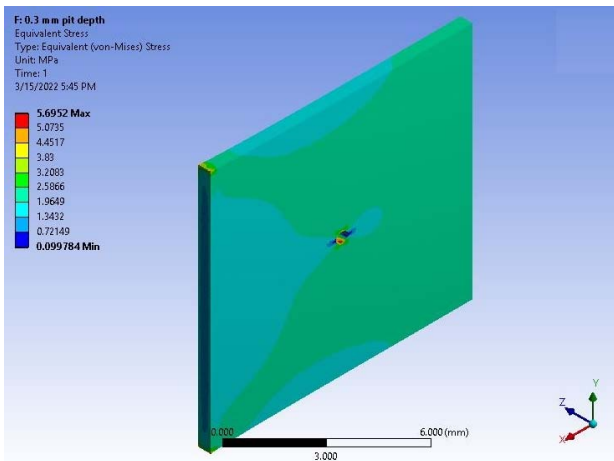
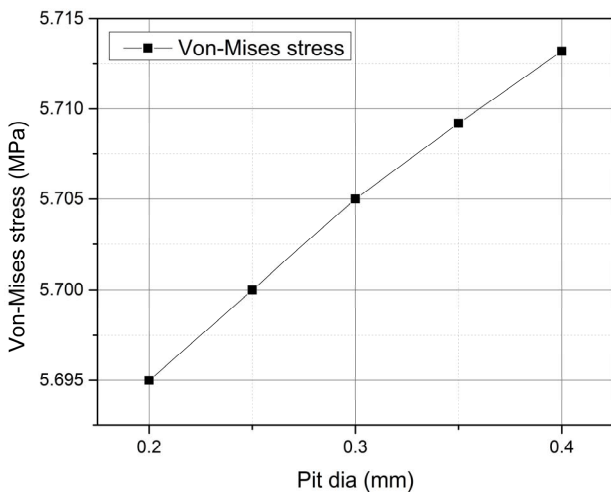


Figure 6. Effect of central pit depth on the stress generated at 0.4 mm pit diameter and 0.5 mm plate thickness

Figure 8 represents the effect of pit diameter on the generated stress in the specimen. A linear trend between the pit diameter along with the correspondingly generated stress was observed. Figure 9 represents the stress distribution on the pit sample with respect to the diameter. The highest stress value was observed to be concentrated at the centre of the pit, indicated by the red colour, while the value of stress decreases upon moving away from the pit.



**Figure 7.** Stress distribution for 0.3 mm central pit depth, 0.4 mm pit diameter and 0.5 mm plate thickness



**Figure 8.** Effect of central pit diameter on stress at 0.3 mm central pit depth and 0.5 mm plate thickness

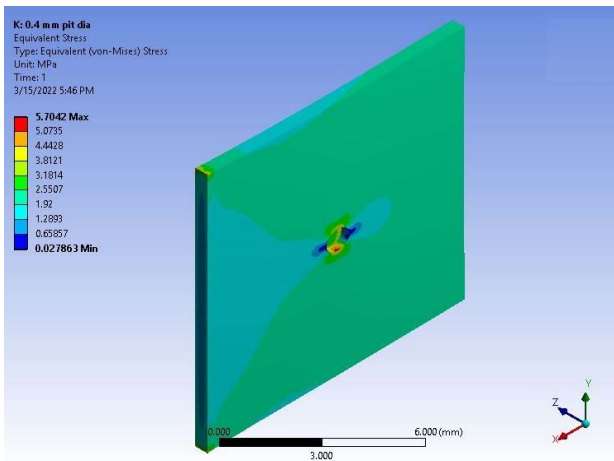


**Figure 9.** Stress distribution for 0.4 mm central pit diameter, 0.3 mm pit depth and 0.5 mm plate thickness

Figure 10 represents the comparative stresses generated by changing the morphology of the pit to a zigzag manner. In comparison with Figures 6 and 8, it was observed that with the changing of pit

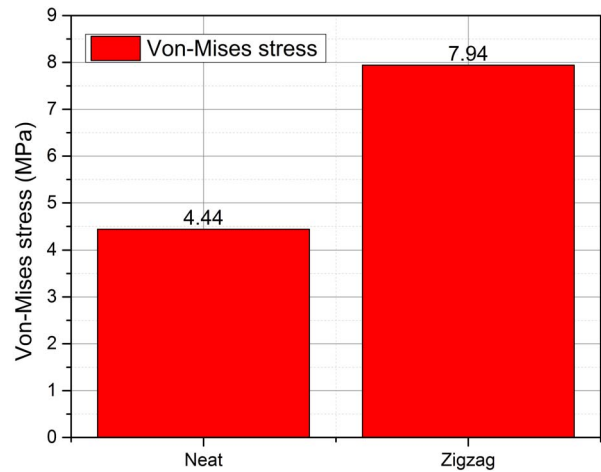


**Figure 10.** Effect of pit morphology on generated stress at 0.4 mm central pit diameter/zigzag width, 0.3 mm depth and 0.5 mm plate thickness

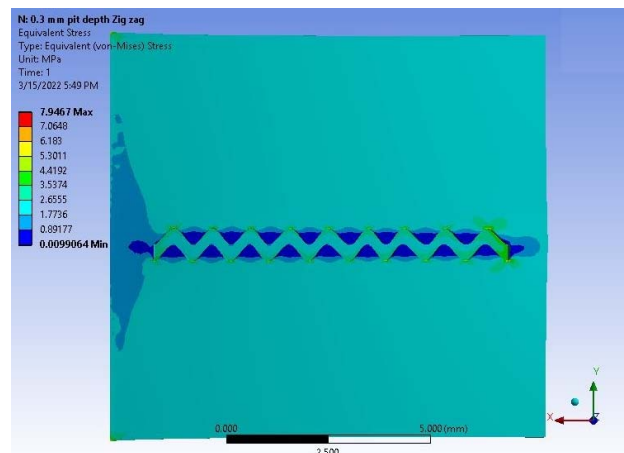
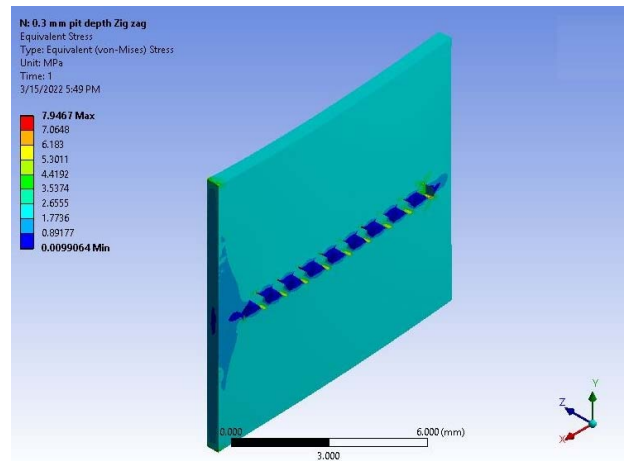


**Figure 11.** Stress distribution for a zigzag pit of 0.4 mm width and 0.3 mm depth and 0.5 mm plate thickness

morphology from circular to zigzag, the quantitative stress has increased tremendously. Figure 11 represents the stress distribution for the changed morphology. It was observed that due to the increase in the number of sharp corners and stress risers, a prominent increase in the overall generated stress was observed along with the

accumulation of stresses at the sharp corners. It is pertinent to mention that it is not a conventional corrosion damage shape. Rather such unconventional morphologies can only arise due to a prolonged combined effect of mechanical degradation (wear, friction, drill, grinding, etc.) and corrosion in some cases.

Figure 12 represents the effect of multiple pits distributed on the specimen having different pit depths. It was observed that due to the increase in the quantity of pits being distributed among the same specimen area, the minute increase in the pit depth resulted in a tremendous increase in the quantitative stress values. Figure 13 represents the stress distribution for the multiple pits. It was observed that the maximum stress was generated at the centre of the respective pits, while the highest stress value was observed for the pits near the respective edges of the specimen.

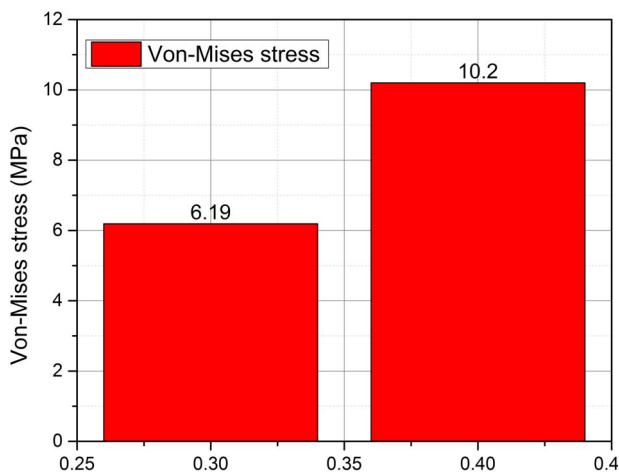


**Figure 12.** Effect of pit depth on generated stress for the effect of multiple distributed pits having 0.4 mm pit diameter

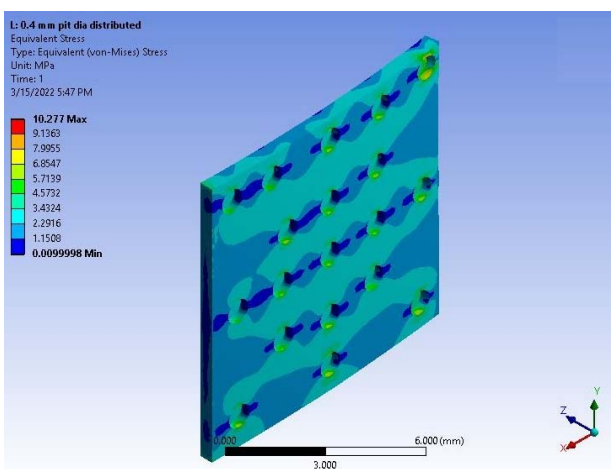


**Figure 13.** Stress distribution for the effect of multiple distributed pits having 0.4 mm pit diameter, 0.3 mm pit depth and 0.5 mm plate thickness at central and random locations

The influence of pitted or crack morphology as per the previously published literature, whose extension has been emphasised in the current work was also compared [11,14]. It was observed that as the pit morphology would change from circular to elliptical or semi-elliptical, the stress concentration factor would increase due to the generation of sharp corners, while the stress concentration would shift from the central region to the corner regions of the pit. This can result in extensive stress magnification, leading up to a 50 % reduction in failure strength, buckling strength and resonant modal frequencies of the structure. The stress generation along with deformation can increase up to 69 and 10 %, respectively due to the pitted structure of the geometry.

Figures 14 and 15 represent the stresses generated against the elliptical pits due to corrosion. It was observed that with the subsequent formation of the pit, the stress rises and is concentrated on the sharp corners of the pit resulting in subsequent stress magnification at a constant force. It was also observed that in comparison to the case where a circular pit of the same area was simulated, the stress was concentrated at the centre of a pit as shown in Figure 9, while as the morphology changes to elliptical, the stress shifts to corner points due to stress concentration and is enhanced accordingly. It was also observed that under the same area for elliptical pits as shown in Figures 14 and 15, the stress concentration increased with the increase in longitudinal and decrease in lateral diameter. This can be attributed to the reduction in the distance between the sharp corners of the elliptical pit, leading to higher stress magnification.

#### 4. Conclusion

The stress generated at constant load when a specimen corrodes due to pitting is directly proportional to the pit diameter and pit depth. Zigzag pit morphologies due to corrosion have the highest stress at the corners of the pattern, while circular pits have the highest stress at the centre of the pit. The zigzag pit morphology has more detrimental effects than circular pits. For multiple distributed pits, the pits closer to the specimen edges exhibit higher stress values than those near the centre of the specimen. The effect of multiple or quantitatively increased number of pits having smaller geometric properties has a more detrimental effect than a single pit with larger

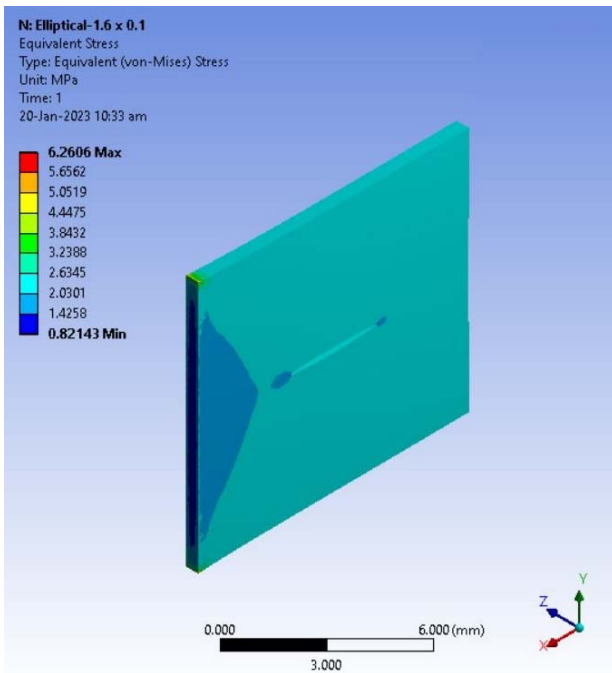


**Figure 14.** Stress distribution for central elliptical pit (0.1 mm longitudinal and 1.6 mm lateral diameter) at 0.3 mm pit depth and 0.5 mm plate thickness

geometric attributes. The formation of elliptical pits is more detrimental than circular pits of the same area as the sharp corners of the elliptical morphology act as stress risers leading to stress magnification. The novelty of this research lies in the convention that typical structural analysis assumes only drills and holes in the structure and not the possibility of pits. This research has focused on the incorporation of the formation and growth of pits in the sample and analysed it based on the corrosion rate calculated using finite element analysis (FEA).

## References

- [1] B. Bobić, A. Vencel, M. Babić, S. Mitrović, I. Bobić, The influence of corrosion on the microstructure of thermally treated ZA27/SiC<sub>p</sub> composites, *Tribology in Industry*, Vol. 36, No. 1, 2014, pp. 33-39.
- [2] X.-g. Huang, J.-q. Xu, 3D analysis for pit evolution and pit-to-crack transition during corrosion fatigue, *Journal of Zhejiang University. Science A*, Vol. 14, No. 4, 2013, pp. 292-299, DOI: [10.1631/jzus.A1200273](https://doi.org/10.1631/jzus.A1200273)
- [3] I. Ahmed, S. Ullah, Z.S. Toor, Design and Fabrication of Stress Corrosion Cracking (SCC) Apparatus and In-situ SCC Study of Heat Treated Aluminum-Copper Alloys, BSc thesis, Department of Materials Science and Engineering, Institute of Space Technology, Islamabad, 2015.

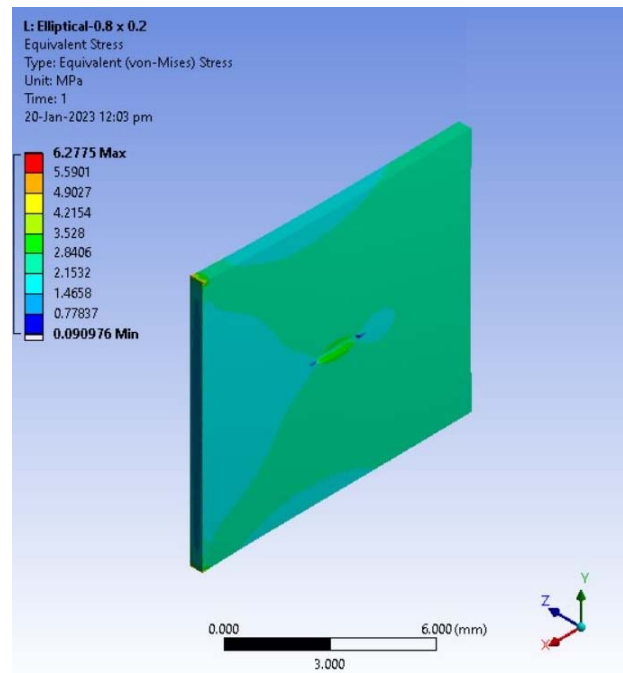


**Figure 15.** Stress distribution for central elliptical pit (0.2 mm longitudinal and 0.8 mm lateral diameter) at 0.3 mm pit depth and 0.5 mm plate thickness

- [4] Z.-y. Han, X.-g. Huang, Y.-g. Cao, J.-q. Xu, A nonlinear cumulative evolution model for corrosion fatigue damage, *Journal of Zhejiang University. Science A*, Vol. 15, No. 6, 2014, pp. 447-453, DOI: [10.1631/jzus.A1200273](https://doi.org/10.1631/jzus.A1200273)
- [5] B. Bobić, S. Mitrović, M. Babić, A. Vencel, I. Bobić, Corrosion behaviour of the as-cast and heat-treated ZA27 alloy, *Tribology in Industry*, Vol. 33, No. 2, 2011, pp. 87-93.
- [6] Z. Wang, X.-y. Jin, N.-g. Jin, X.-l. Gu, C.-q. Fu, Cover cracking model in reinforced concrete structures subject to rebar corrosion, *Journal of Zhejiang University. Science A*, Vol. 15, No. 7, 2014, pp. 496-507, DOI: [10.1631/jzus.A1300393](https://doi.org/10.1631/jzus.A1300393)
- [7] W.-l. Jin, Y.-x. Zhao, Effect of corrosion on bond behavior and bending strength of reinforced concrete beams, *Journal of Zhejiang University. Science A*, Vol. 2, No. 3, 2001, pp. 298-308, DOI: [10.1007/BF02839464](https://doi.org/10.1007/BF02839464)
- [8] J.H. Ri, R.G. Ripeanu, Evaluation of the wear and corrosion resistance of coated parallel gate valve, *Tribology and Materials*, Vol. 1, No. 1, 2022, pp. 11-20, DOI: [10.46793/tribomat.2022.002](https://doi.org/10.46793/tribomat.2022.002)
- [9] Z.S. Toor, I. Ahmed, S. Ullah, A.N. Butt, S.W. Hussain, Influence of ageing time and stress on corrosion behavior of AA2024-T6 in saturated NaCl solution, *Journal of Space Technology*, Vol. 8, 2018, pp. 38-44.
- [10] A. Sagalovych, V. Sagalovych, V. Popov, S. Dudnik, O. Olijnyk, Tribological characteristics of samples made from titanium alloy VT5 nitrated in plasma glow discharge, *Tribology and*

- Materials, Vol. 1, No. 3, 2022, pp. 106-113, DOI: [10.46793/tribomat.2022.013](https://doi.org/10.46793/tribomat.2022.013)
- [11] Z.S. Toor, Parametric optimization using finite element analysis based virtual framework, Journal of Space Technology, Vol. 12, 2022, pp. 1-5.
- [12] Z.S. Toor, Influence of crack morphology and its distribution on stress magnification of AA2024-T3, Journal of Space Technology, Vol. 10, 2020, pp. 50-57.
- [13] Z.S. Toor, A.H. Baluch, A. Wadood, A.U. Rehman, M. Saleem, M.S. Butt, K. Hayat, Impact based characterization of composites using a computational framework, Acta Astronautica, Vol. 202, 2023, pp. 705-714, DOI: [10.1016/j.actaastro.2022.11.011](https://doi.org/10.1016/j.actaastro.2022.11.011)
- [14] Z.S. Toor, Effect of drill on mechanical and modal characteristics of aluminum sheet, Journal of Space Technology, Vol. 11, 2021, pp. 14-19.
- [15] M. Shifa, F. Tariq, F. Khan, Z.S. Toor, R.A. Baloch, Towards light weight multifunctional hybrid composite housing for satellite electronics, Materials Research Express, Vol. 6, No. 12, 2019, Paper 125629, DOI: [10.1088/2053-1591/ab6928](https://doi.org/10.1088/2053-1591/ab6928)
- [16] S.H. Zaferani, The application of finite element analysis as a new approach in corrosion and integrity assessment programs, International Journal of Petrochemical Science & Engineering, Vol. 2, No. 1, 2017, pp. 18-20, DOI: [10.15406/ipcse.2017.02.00026](https://doi.org/10.15406/ipcse.2017.02.00026)
- [17] S. Zeng, S. Gu, S. Ren, Y. Gu, C. Kong, L. Yang, A modeling method for finite element analysis of corroded steel structures with random pitting damage, Buildings, Vol. 12, No. 11, 2022, Paper 1793, DOI: [10.3390/buildings12111793](https://doi.org/10.3390/buildings12111793)
- [18] Z.-q. Zhang, Y.-l. Li, X.-y. Zhu, X.-h. Liu, Meso-scale corrosion expansion cracking of ribbed reinforced concrete based on a 3D random aggregate model, Journal of Zhejiang University. Science A, Vol. 22, No. 11, 2021, pp. 924-940, DOI: [10.1631/jzus.A2100304](https://doi.org/10.1631/jzus.A2100304)
- [19] Q. Feng, G.-n. Wang, Y.-p. Zhang, R.-q. Xu, Numerical simulation of partial-interaction load-deflection behavior of corroded reinforced concrete beams based on a segmental approach and evaluation of reinforcement corrosion level, Journal of Zhejiang University. Science A, Vol. 21, No. 4, 2020, pp. 280-293, DOI: [10.1631/jzus.A1900616](https://doi.org/10.1631/jzus.A1900616)
- [20] S. Pal, Simulation of finite element model of surface pit on F304 stainless steel, Journal of Mechanical and Mechanics Engineering, Vol. 5, No. 3, 2019, pp. 1-12.